

# Oscillating kink behavior in a traversable wormhole

Tian-Chi Ma<sup>1,\*</sup> and Hai-Qing Zhang<sup>1,2,†</sup>

<sup>1</sup>*Center for Gravitational Physics, Department of Space Science,  
Beihang University, Beijing 100191, China*

<sup>2</sup>*Peng Huanwu Collaborative Center for Research and Education,  
Beihang University, Beijing 100191, China*

We investigate the time evolution of spherically symmetric radial domain walls (kinks) in the background of a two-way traversable Simpson-Visser wormhole. By numerically solving the scalar-field equation with a double-well potential, we show that the wormhole throat parameter  $a$  has a strong impact on the dynamics of the radial kink: larger  $a$  leads to wider throats and allows the domain wall to oscillate across the throat with large amplitude, whereas smaller  $a$  confines the motion nearby the throat. In addition, each time the kink crosses the wormhole throat, it emits scalar wave packets, causing its oscillation amplitude to gradually decrease. Our results reveal how the wormhole geometry influences the motion of defects and their energy transfer, providing new insights into the dynamics of topological defects in exotic spacetime.

## I. INTRODUCTION

In field theories with spontaneous symmetry breaking, the causal disconnection between different regions of the system allows each region to select a different vacuum state. Topological defects then naturally emerge at the boundaries between these regions [1–3]. Depending on the class of symmetry being broken, different classes of defects, such as monopoles, cosmic strings, and domain walls may emerge [4–6]. Domain walls (also commonly referred to as kinks) arise from the spontaneous breaking of  $Z_2$  symmetry. They exhibit a step-like structure in which the scalar field undergoes a sharp transition from one vacuum to the other, leading to a localized concentration of energy density at the interface. Owing to their extended nature and relatively high tension, domain walls can induce significant gravitational effects and play an important role in early-universe cosmology, phase transitions, and nonperturbative field dynamics [7–9]. Domain walls are also often considered potential candidates for dark matter or other intriguing structures [10–12]. Fundamental constants, such as particle masses and the fine-structure constant and etc., may vary upon crossing a domain wall [13–15]. Since domain walls can alter fundamental physical constants, scientists have developed various experiments to detect them, including satellite synchronization [16–19], electric dipole moment measurements [20], magnetometry [21, 22], acceleration induced by mass differences [23], and gravitational wave detectors [24–26]. Therefore, studying domain walls or kinks in gravitational systems is a task of considerable importance.

The evolution of domain walls in flat spacetime has been extensively studied, including in both 2+1 and 3+1 dimensions. Reference [27] examines the dynamical evolution of both planar

---

\* [tianchima@buaa.edu.cn](mailto:tianchima@buaa.edu.cn)

† [hqzhang@buaa.edu.cn](mailto:hqzhang@buaa.edu.cn)

and radial kinks in Klein–Gordon models, with a particular focus on their existence and stability properties. The attractive interaction between a kink and an antikink has been analyzed in Ref. [28], where an effective model was constructed via the variational approximation, yielding results in agreement with those from the full dynamical model. In Ref. [29], the influence of radial perturbations on kink configurations is studied, and the possibility of extracting energy from the kink is explored. More recently, some studies have employed the gauge/gravity duality [30, 31] to probe the statistical behavior of kinks in the strongly coupled regime of the boundary field theory [32, 33]. Additional related work can be found in references [34–39].

In this context, an interesting question arises: compared with flat spacetime, what characteristic features does the kink exhibit in curved spacetime? Compact astrophysical objects, including black holes [40, 41], neutron stars [42, 43], boson stars [44, 45], and wormholes [46–48], serve as natural laboratories for studying the nonlinear behavior of fields under strong gravity. Compared with flat spacetime, the behavior of domain walls in curved geometry is significantly richer due to the background curvature, horizons, and the diverse structures of spacetime topology. In black hole backgrounds, scientists have conducted several studies on domain walls, including their stationary and transient behaviors. Studies have shown that black holes exhibit a repulsive effect on static thick domain walls [49–52]. In addition, when a kink passes near a black hole, it displays behavior resembling ringdown modes [53]. Recently, scientists have extended the study of kink dynamics to compact stars, such as neutron stars and boson stars. They found that compact stars can slow down the motion of kinks and may even produce a rebound-like effect on them [54, 55].

However, studies of kinks in wormhole backgrounds remain very limited, with current research mostly focusing on static configurations and perturbative analyses [56–60]. A wormhole refers to a tunnel-like spacetime structure that links two distant or otherwise disconnected regions. The earliest wormhole solution, known as the Einstein–Rosen bridge, was proposed by Einstein and Rosen [61]. Since this type of wormhole is non-traversable, it was long considered merely a mathematical construction rather than a physically realizable entity. Many years later, Ellis obtained a new wormhole solution, and Morris and Thorne subsequently proved that the Ellis wormhole is traversable, such that matter or light signals can safely pass through the wormhole without encountering horizons or singularities [62, 63]. The existence of traversable wormholes requires matter that violates classical energy conditions, known as “exotic matter”, whose negative energy density can support the wormhole throat against collapse [64, 65]. For further studies on wormholes, see Refs. [66–75].

Moreover, in traversable wormholes, the two asymptotically flat regions may be interpreted as separate universes. In such setups, a kink located in one universe could, in principle, travel through the wormhole throat and enter the other universe. The arrival of such a high-tension defect could substantially alter the local gravitational environment, disrupt astrophysical systems, or leave observable imprints in cosmology. Therefore, studying the evolution of kinks in wormhole spacetimes has significant theoretical and even practical importance. To our knowledge, the present work constitutes the first detailed study of the spherically symmetric radial kink dynamics in the background of a traversable wormhole.

In this paper, we investigate the time evolution of radial domain walls in the background of the Simpson-Visser two-way traversable wormholes. In Sec. II, we introduce the Simpson-Visser spacetime and the spherically symmetric scalar-field model with a double-well potential. In Sec. III, we numerically solve the scalar field equation to investigate how the width of the

wormhole throat affects the dynamical evolution of the kink, as well as the mechanism by which the kink transfers energy to the background. Finally, we draw conclusions and discussions in Sec. IV. Throughout this work, we adopt geometric units  $G = c = 1$  and the metric signature  $(-, +, +, +)$ .

## II. THEORETICAL FRAMEWORK

### A. Simpson-Visser spacetime and wormhole configurations

The Simpson-Visser spacetime can be described by the line element presented in [76],

$$ds^2 = -A(r) dt^2 + \frac{1}{A(r)} dr^2 + (r^2 + a^2) (d\theta^2 + \sin^2 \theta d\varphi^2), \quad (1)$$

$$A(r) = 1 - \frac{2M}{\sqrt{r^2 + a^2}}, \quad (2)$$

where  $M$  is the ADM mass while  $a$  is the characteristic parameter of this spacetime. The coordinate range of this spacetime is

$$t \in (-\infty, +\infty); \quad r \in (-\infty, +\infty); \quad \theta \in [0, \pi]; \quad \phi \in [0, 2\pi). \quad (3)$$

By changing the parameter  $a$ , this spacetime can exhibit four different scenarios:

- (1) The ordinary Schwarzschild spacetime for  $a = 0$ ;
- (2) A regular black hole geometry with a one-way *spacelike* throat for  $2M > a > 0$ ;
- (3) A one-way wormhole geometry with an extremal *null* throat for  $a = 2M$ ;
- (4) A canonical traversable wormhole geometry with a two-way *timelike* throat for  $a > 2M$ .

In this work, we focus on the last scenario by studying the time evolution of radial kinks in the background of two-way traversable wormholes. Therefore, in the following parts of this article, we restrict our analysis to the case with  $a > 2M$ .

To better illustrate the geometry and properties of the two-way traversable wormhole, we take advantage of the embedding diagrams. Specifically, we fix the time  $t = \text{const.}$  and  $\theta = \pi/2$ , and then embed a two-dimensional spatial hypersurface of the wormhole spacetime into three-dimensional Euclidean space. This allows the intrinsic properties of the wormhole spacetime to be intuitively displayed. By introducing cylindrical coordinates  $(\rho, \varphi, z)$ , the metric on this two-dimensional hypersurface can be expressed as

$$\begin{aligned} ds^2 &= \frac{1}{A(r)} dr^2 + (r^2 + a^2) d\varphi^2 \\ &= d\rho^2 + dz^2 + \rho^2 d\varphi^2. \end{aligned} \quad (4)$$

Comparing the two equations above, we then obtain the expression for  $\rho$  and  $z$  as

$$\rho(r) = \sqrt{r^2 + a^2}, \quad z(r) = \int_0^r \sqrt{\frac{1}{A(r)} - \left(\frac{d\rho}{dr}\right)^2} dr. \quad (5)$$

In Fig. 1, we present a set of metric functions  $A(r)$  and embedding diagrams  $z(\rho)$  corresponding to different values of  $a$ . In Fig. 2, we show the 3D rotational plots of the embedding

function  $z(\rho)$  for  $a = 9M$  and  $a = 2.02M$  from panel (b) of Fig. 1. It can be intuitively seen that the embedding diagram of the wormhole is divided into two symmetric halves about  $z = 0$  plane, resembling two funnels that are joined at their narrowest ends. The upper and lower halves correspond to  $r > 0$  and  $r < 0$ , respectively. The narrowest part is referred to as the throat of the wormhole (corresponding to  $z = 0$ ). It is observed from Fig. 1(a) that for larger values of the parameter  $a$ , the metric function  $A(r)$  exhibits a shallower valley, and correspondingly, the embedding diagram has a wider throat. Conversely, for smaller values of  $a$ , the metric function  $A(r)$  shows a deeper valley, corresponding to a narrower throat.

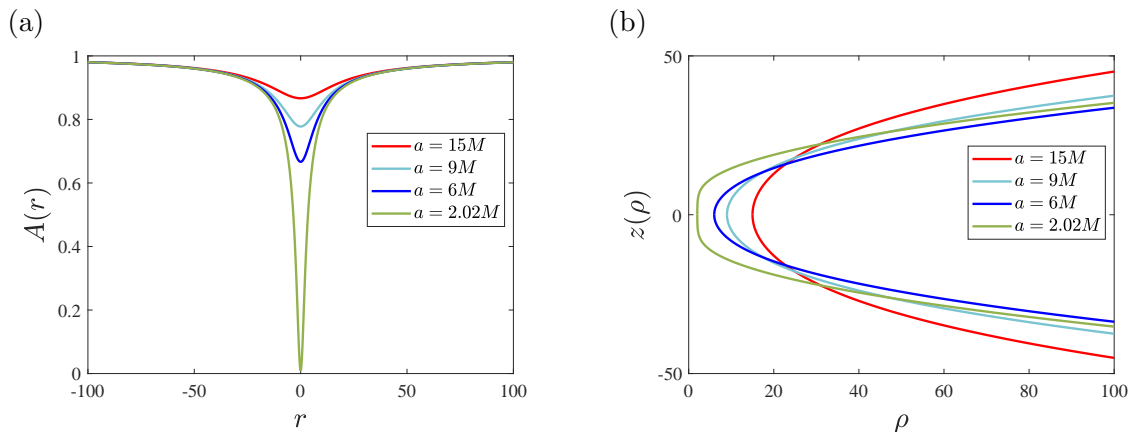


FIG. 1: The metric function  $A(r)$  and the embedding function  $z(\rho)$  with four different values of  $a$ , i.e.,  $a = 15M$ ,  $a = 9M$ ,  $a = 6M$  and  $a = 2.02M$ .

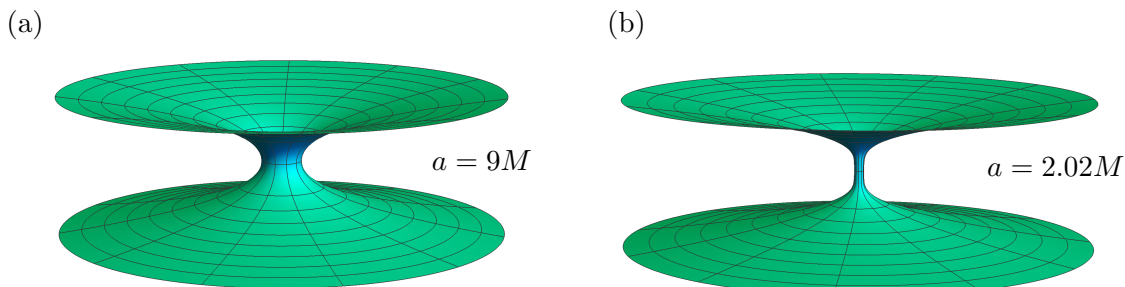


FIG. 2: Three-dimensional plot of rotations of the embedding function  $z(\rho)$  along  $\rho = 0$ , with panel (a) and panel (b) corresponding to  $a = 9M$  and  $a = 2.02M$ , respectively.

## B. Radial kink model

In order to study the evolution of kinks in the background of the two-way traversable wormholes, we consider a real scalar field  $\phi$  with the action

$$S = \int d^4x \sqrt{-g} \left[ \frac{1}{2} g_{\mu\nu} \nabla^\mu \phi \nabla^\nu \phi + V(\phi) \right], \quad (6)$$

where we will adopt the metric  $g_{\mu\nu}$  as in Eq. (1), and the potential  $V(\phi)$  is a double-well potential

$$V(\phi) = \frac{1}{4}(\phi^2 - 1)^2, \quad (7)$$

which has minimums at  $\phi = \pm 1$ . Therefore, after breaking the  $Z_2$  symmetry in the action (6), the scalar field  $\phi$  will settle down to  $\phi = +1$  or  $\phi = -1$ , which will in turn form the solutions of kinks [13, 77–79]. The equation of motion for the scalar field  $\phi$  reads

$$-\frac{1}{\sqrt{-g}} \partial_\mu (\sqrt{-g} g^{\mu\nu} \partial_\nu \phi) + \frac{\delta V(\phi)}{\delta \phi} = 0. \quad (8)$$

In this work, we are interested in the time evolution of the spherically symmetric kink in the background of the two-way traversable wormholes. Specifically, in the background of the spherical geometry, the Eq. (8) can be re-expressed as

$$\begin{aligned} \partial_t^2 \phi - \frac{1}{r^2 + a^2} A(r) \partial_r ((r^2 + a^2) A(r) \partial_r \phi) - \frac{1}{(r^2 + a^2) \sin \theta} A(r) \partial_\theta (\sin \theta \partial_\theta \phi) \\ - \frac{1}{(r^2 + a^2) \sin^2 \theta} A(r) \partial_\varphi^2 \phi + A(r) \phi^3 - A(r) \phi = 0. \end{aligned} \quad (9)$$

Due to the spherical symmetry of the system, the polar and azimuthal angular derivative terms in the equation do not play a role. Therefore, we can simplify the configurations of the kink to only depend on time  $t$  and the radial direction  $r$ . Hence we dub it as “*radial kinks*”.

### III. RADIAL KINKS IN THE SIMPSON-VISSER WORMHOLES

In this section we will study the evolution of kinks in the background of the Simpson-Visser wormholes. The dynamics of kinks are governed by the Eq. (9). The initial configuration of the kink can be given by [80],

$$\phi(0, r) = \tanh \left[ \frac{r - r_k(0)}{\sqrt{2(1 - v^2)}} \right], \quad (10)$$

where  $r_k(0)$  is the initial position of the kink at  $t = 0$  while  $v$  represents the initial velocity of the kink. Throughout the paper, we always set  $v = 0$ . This means that within the framework of the field model described by Eq. (9), we assume initial conditions of the kink with a given radius and zero initial velocity. The position of the kink  $r_k$  is defined at the transition that  $\phi$  changes its sign, i.e.,  $\phi(t, r_k) = 0$ .

In numerics, we set the radial direction  $r \in [-100, 100]$  and we discretize it into 5000 grid points. At the boundary of  $r = \pm 100$ , we impose the Dirichlet boundary condition of the scalar field  $\phi(t, \pm 100) = \pm 1$ . This requirement is consistent with the initial condition. Besides, we employ the fourth-order Runge-Kutta method in the time direction with a time step of  $\Delta t = 0.02$ . In the radial direction  $r$ , we used the sixth-order difference method with  $\Delta r = 0.04$ . To check the numerical stability, we also tested other time and spatial step sizes, such as  $\Delta t = 0.04$ ,  $\Delta r = 0.08$  or  $\Delta t = 0.01$ ,  $\Delta r = 0.02$ , and obtained consistent results.

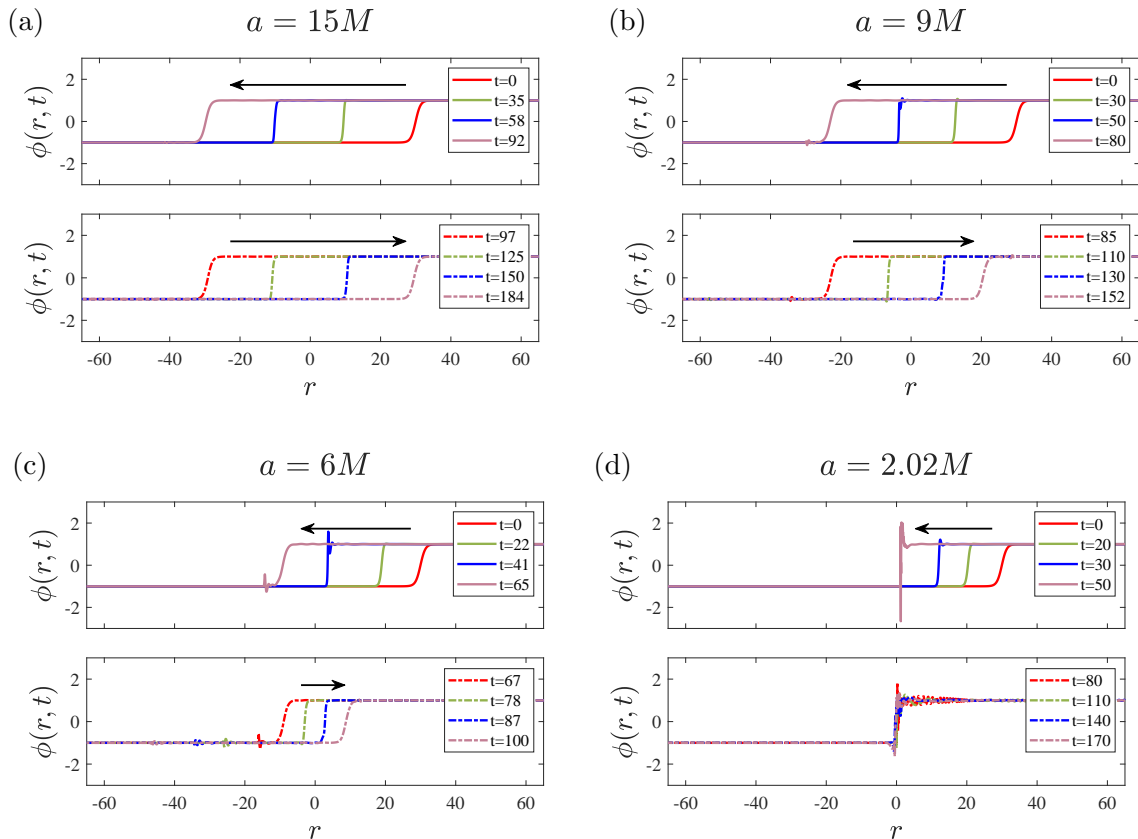


FIG. 3: Time evolution of the scalar field  $\phi$  in the wormhole background with four different values of  $a$ . In each panel, the scalar field shares the same initial configuration of the kink position at  $r_k(0) = 30$ . Each panel is divided into two smaller parts, in which the solid line (in the upper part) represents the kink moving leftwards, while the dashed line (in the lower part) represents the kink moving rightwards. However, in the panel (d) we can see that in the lower part the dashed lines are confined nearby the throat of the wormhole. The black arrows in each panel represent the moving direction of the kinks.

### A. Time evolution of the radial kink

Fig. 3 shows the time evolution of the radial kink for four different values of the parameter  $a$  with  $a = 15M$ ,  $a = 9M$ ,  $a = 6M$  and  $a = 2.02M$ , respectively. (In numerics we scaled  $M = 1$ .) In each panel, we use the same initial scalar field configuration, with the kink located at  $r = 30$ . From the figure, it is clear that for larger values of  $a$  (e.g.,  $a = 15M$ ), the kink starts moving leftward from  $r = 30$ , reaches a maximum displacement at  $r \approx -29.83$  ( $t = 92$ ) on the opposite side of the wormhole, and then reverses the direction to move rightward, reaching up to  $r \approx 29.47$  ( $t = 184$ ). It should be noted that, after the time  $t = 184$  the kink reverses its direction again to move leftward and repeat its evolution back and forth. The back-and-forth movement of the kink between the two sides of the wormhole may help people (if he lives in one part of the wormhole) to retrieve information from the other part of the wormhole. The oscillating behavior of kinks will be studied in detail later.

For smaller values of  $a$  (e.g.,  $a = 6M$ ), the kink starts from its initial position at  $r = 30$  as well, then it moves leftward until  $r \approx -9.26$  ( $t = 65$ ), and then moves rightward to around  $r \approx 8.70$  ( $t = 100$ ). Compared to the case of  $a = 9M$ , we observed that for larger values of  $a$

(with a wider wormhole throat), the kink has a larger range of motion. As  $a$  is very close to the critical value  $a = 2M$ , as shown in the panel (d) of Fig. 3 with  $a = 2.02M$ , the kink's motion is finally confined to an extremely narrow region around the throat of the wormhole, rather than going through the wormhole. This is consistent with the fact that as  $a \leq 2M$ , the wormhole will become a null or one-way spacelike throat. Additionally, another important feature worth noting is that, as shown in panels (b)-(d) in Fig. 3, ripples are generated as the kink traverses through the throat. We will investigate this wave packet shedding in the next subsection III B.

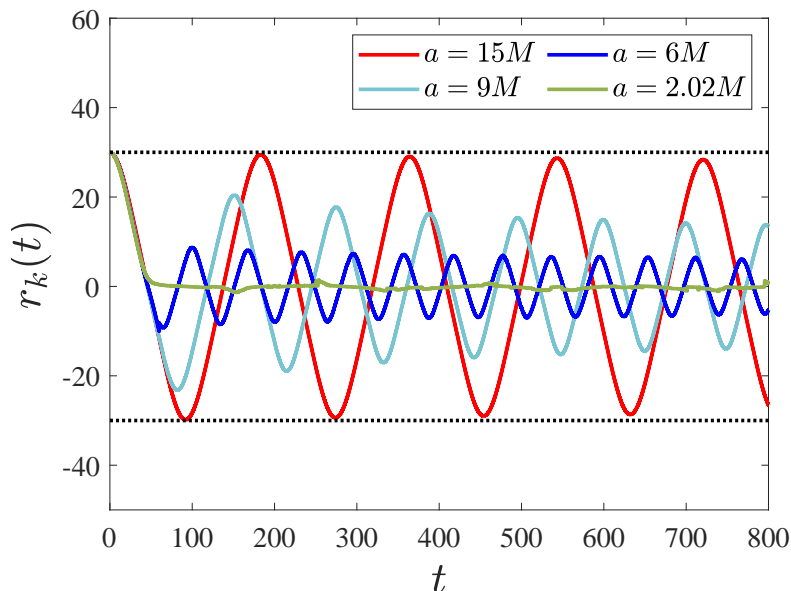


FIG. 4: Time evolution of the kink's position  $r_k(t)$  with four different values of the parameter  $a$ . In order to better illustrate the evolutions of the kink position, two dotted lines at  $r_k = \pm 30$  have been added as a reference.

In Fig. 4 we show the time evolution of the kink's position  $r_k(t)$  over a much longer time<sup>1</sup>. It is evident that the kink oscillates back and forth between the two sides of the wormhole, with the oscillation amplitude decreasing over time. For smaller values of  $a$ , the reduction in oscillation amplitude becomes more pronounced. This behavior reminds us of the dynamics of a damped oscillator, although quantitatively this behavior does not fully align with that of a damped oscillator. We will provide a more detailed explanation and analysis of this behavior in the next subsection III B.

### B. Wave packets shedding and energy transfer

In the preceding subsection we have observed the ripples appeared in the scalar fields as shown in the panels (b)-(d) in Fig. 3. These ripples usually turn out as they approach the throat of the wormhole. Therefore, these ripples must come from the interactions of the kinks to the wormhole throat. Besides, our previous results also show that the amplitude of the kink's

<sup>1</sup> Actually it is hard to track the position of the kink for the case of  $a = 2.02M$ , since there are many complex oscillatory modes superimposed on the kink. Therefore, in Fig. 4, the curve corresponding to  $a = 2.02M$  takes the averagely approximate range of the kink's location. The full time animations of the kink evolution can be found in this [link](#).

motion decreases over time, indicating that the energy of the kink reduces over time. In order to study this phenomenon, we will perform a further analysis by using the case of  $a = 9M$  as an example.

The energy density of the system  $\mathcal{H}$  can be obtained through the Legendre transformation of the Lagrangian  $\mathcal{L}$ ,

$$\begin{aligned}\mathcal{H}(\Pi, \phi) &= \frac{1}{\sqrt{h}}(\Pi\dot{\phi} - \sqrt{-g}\mathcal{L}) \\ &= \frac{\Pi^2\sqrt{-g_{tt}}}{2gg^{tt}} + \frac{1}{2}\sqrt{-g_{tt}}h^{ab}\partial_a\phi\partial_b\phi + \sqrt{-g_{tt}}V(\phi).\end{aligned}\quad (11)$$

where  $\Pi = -\sqrt{-g}g^{tt}\dot{\phi}$  is the canonical momentum, and  $h^{ab}$  is the induced metric on the three-dimensional spacelike hypersurface at a fixed time  $t$ .

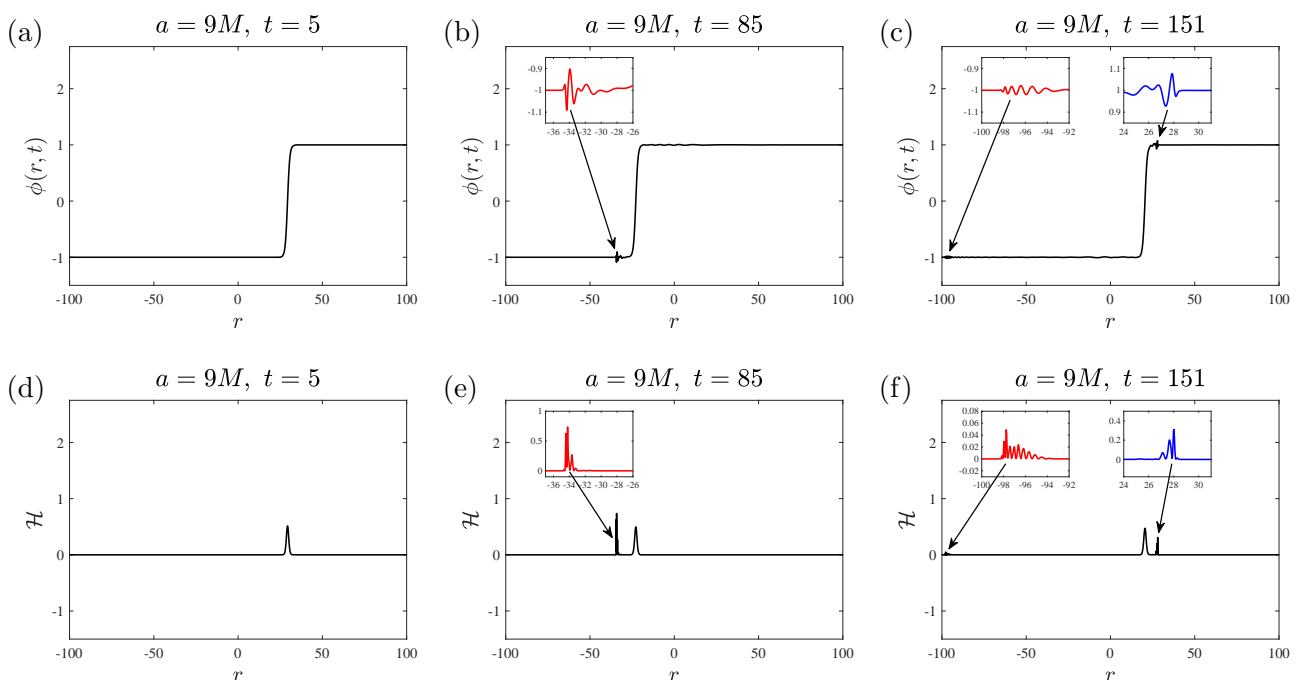


FIG. 5: Configurations of the scalar field  $\phi$  and its corresponding energy density  $\mathcal{H}$  at different times, i.e.,  $t = 5, 85,$  and  $151$ . The initial position of the kink is  $r_k(0) = 30$ , and the throat parameter is  $a = 9M$ . The inset plots are the enlarged version of the wave packets or the energy densities as the arrows indicate.

In the panels (a)-(c) of Fig. 5, we show the configurations of the scalar field  $\phi$  at three different times for  $a = 9M$ . Meanwhile, in the panels (d)-(f) of Fig. 5, we exhibit their corresponding energy densities  $\mathcal{H}$ , respectively. At  $t = 5$  (see the panels (a) and (d) of Fig. 5), the kink just starts from its original location and moves towards the wormhole, but has not yet arrived at the wormhole throat. It can be observed that at this time there are no ripples in the scalar fields. Besides, the energy density peaks at the kink location, while the energy density is vanishing at all other positions. This is because the scalar field  $\phi$  exhibits a step-like profile at the kink, which contributes the most excited energy to the kink. In contrast, at other positions the scalar field is flat, which stays in its lowest energy state.

At  $t = 85$  (see the panels (b) and (e) of Fig. 5), the kink passes through the throat once. It can be observed that the field configuration and energy density at  $t = 85$  differ significantly

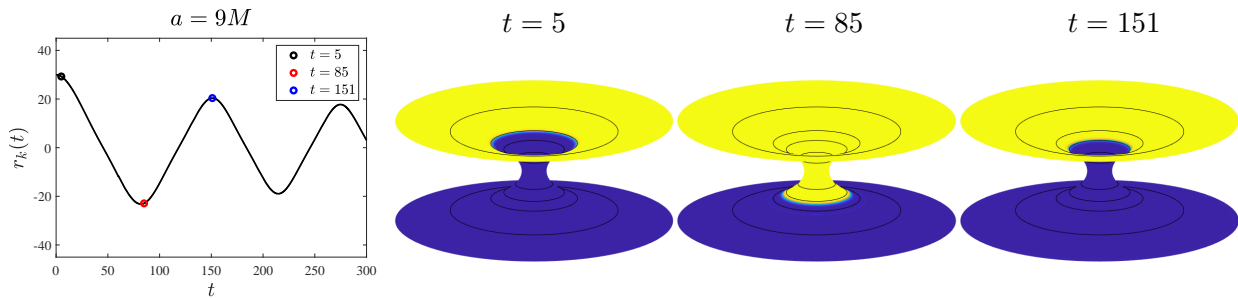


FIG. 6: The time evolution of the position of the radial kink for  $a = 9M$ . On the most left panel, the black, red, and blue circles represent the exact positions of the kinks in panels (a), (b), and (c) of Fig. 5, respectively. The amplitude of the oscillation decreases due to the interactions between the scalar field and the throat. The three panels on the right are the 3D versions of the kinks corresponding to the indicated times in the left panel.

from those at  $t = 5$ . In panel (b), aside from the kink, a wave packet is present at around  $r \approx -34$  (see the inset plot for enlarged details). This wave packet shedding from the kink profile comes from the interactions between the kink and the throat. Therefore, the energy of the kink will decrease after it passes through the throat. This in turn causes the amplitude of the  $r_k(t)$  to decrease, just as shown in the most left panel in Fig. 6. In the meantime, in panel (e) of Fig. 5, except for a peak of the energy density at the location of the kink, there also exists an excitation of energy density at the positions of the excited wave packet.

Afterwards, the kink will turn its direction to move towards the throat again. However, the shedding wave packet will continue moving leftwards. This phenomenon can be clearly seen in the panels (c) and (f) in Fig. 5 at time  $t = 151$ . Now, the kink already passed through the throat twice. There appears another new generated wave packet at around  $r \approx 28$ , which is represented by the blue inset plot in panel (c). This wave packet is due to the interactions between the scalar field and the wormhole throat. The wave packet in red inset plot in panel (c) is from the wave packet in panel (b), which has propagated leftwards to  $r \approx -97$  at time  $t = 151$ . The amplitudes of the wave packet in panel (c) is smaller than that in panel (b), since the wave packet has dissipated into space during the propagations. The corresponding energy densities of the kinks and two wave packets are shown in panel (f). Later, similar behaviors will continue in the subsequent time evolution of the scalar field. That is, each time the kink passes through the wormhole throat, there will emit a wave packet into the background, transferring the energy to the background. Consequently, the amplitude of the kink's motion will gradually decrease, as shown in the most left panel of Fig. 6.

In Fig. 6 we exhibit the time evolution of the locations of the kinks for  $a = 9M$  and the 3D version of the kinks for three specific times, i.e.,  $t = 5, 85$  and  $151$ . In the most left panel we find that the amplitude of the oscillation decreases in time, due to the shedding wave packets from the interactions of the kink with the wormhole throat. On the right side panels, we show the 3D version of the kinks at three specific times. The yellow parts correspond to the kink with value  $\phi = +1$  while the dark blue parts correspond to  $\phi = -1$ . The full animations of the kink evolutions can be found in this [link](#).

#### IV. CONCLUSIONS AND DISCUSSIONS

In this work, we studied the evolutions of the radial kinks in the background of a traversable Simpson-Visser Wormhole. We have realized the oscillatory behavior of the kinks which can traverse through the two sides of the wormholes. Our results show that the wormhole throat parameter  $a$  has a decisive influence on the motion of the spherically symmetric radial kink. That is, larger values of  $a$  lead to a wider throat, allowing the kink to oscillate between the two asymptotically flat regions with a larger amplitude, whereas smaller values of  $a$  confine the kink to oscillate with a smaller amplitude. In particular, as  $a$  approaches the critical value  $a = 2M$ , the throat becomes an extremal null throat, which confines the kink inside the throat. It is worth noting that the oscillating behavior of kinks between the two sides of the wormhole may help people to extract the information from the other side of the wormhole.

Due to the fact that the topology of the wormhole differs from that of ordinary compact stars, a single radial kink is protected by the wormhole topology and does not disappear at late times. Each time the radial kink passes through the wormhole throat, it transfers energy to the background in the form of emitted wave packets, thereby reducing its own energy and causing its oscillation amplitude to gradually decrease. This only drives the kink to oscillate within a progressively smaller region near the throat, while the kink itself persists throughout the evolution. In contrast, in the backgrounds of boson stars and neutron stars, the kink ultimately transfers all of its energy to the background through oscillations, and eventually the kink disappears into the background [54, 55].

Of course, the present work represents only a small step in this line of research. The wormhole background considered here is symmetric, the evolution of kinks in asymmetric wormholes deserves to be studied in future work. Our work can also be extended to axially symmetric wormholes, in order to explore the influence of angular momentum on kink dynamics. Finally, we emphasize one nontrivial observational feature revealed in this study: when the radial kink traverses the wormhole throat, it emits wave packets and radiates energy into the background in a regular manner. This phenomenon may be useful for observational searches of wormholes and for distinguishing wormholes from other compact stellar objects.

#### ACKNOWLEDGEMENTS

This work was partially supported by the National Natural Science Foundation of China (Grants No.12175008).

- 
- [1] R. H. Brandenberger, “Topological defects and structure formation,” *International Journal of Modern Physics A*, vol. 9, no. 13, pp. 2117–2189, 1994.
  - [2] J. C. Teo and T. L. Hughes, “Topological defects in symmetry-protected topological phases,” *Annual Review of Condensed Matter Physics*, vol. 8, no. 1, pp. 211–237, 2017.
  - [3] J. M. Kosterlitz, “Nobel lecture: Topological defects and phase transitions,” *Reviews of Modern Physics*, vol. 89, no. 4, p. 040501, 2017.
  - [4] L. M. Pismen, *Vortices in nonlinear fields: From liquid crystals to superfluids, from non-equilibrium patterns to cosmic strings*, vol. 100. Oxford University Press, 1999.

- [5] N. Manton and P. Sutcliffe, *Topological solitons*. Cambridge University Press, 2004.
- [6] Y. M. Bunkov and H. Godfrin, *Topological defects and the non-equilibrium dynamics of symmetry breaking phase transitions*, vol. 549. Springer Science & Business Media, 2000.
- [7] T. W. B. Kibble and G. In, “Phase transitions in the early universe,” *Quantum Structure of Space and Time*, p. 391, 1982.
- [8] A. Vilenkin, A. Vilenkin, and E. Shellard, *Cosmic strings and other topological defects*. Cambridge University Press, 1994.
- [9] T. Vachaspati, *Kinks and domain walls: An introduction to classical and quantum solitons*. Cambridge University Press, 2006.
- [10] W. H. Press, B. S. Ryden, and D. N. Spergel, “Dynamical evolution of domain walls in an expanding universe,” *Astrophysical Journal, Part 1 (ISSN 0004-637X)*, vol. 347, Dec. 15, 1989, p. 590-604. *Research supported by NASA and Alfred P. Sloan Foundation.*, vol. 347, pp. 590–604, 1989.
- [11] P. Avelino, C. Martins, J. Menezes, R. Menezes, and J. Oliveira, “Dynamics of domain wall networks with junctions,” *Physical Review D—Particles, Fields, Gravitation, and Cosmology*, vol. 78, no. 10, p. 103508, 2008.
- [12] A. Friedland, H. Murayama, and M. Perelstein, “Domain walls as dark energy,” *Physical Review D*, vol. 67, no. 4, p. 043519, 2003.
- [13] T. W. Kibble, “Topology of cosmic domains and strings,” *Journal of Physics A: Mathematical and General*, vol. 9, no. 8, p. 1387, 1976.
- [14] A. Vilenkin and A. E. Everett, “Cosmic strings and domain walls in models with goldstone and pseudo-goldstone bosons,” *Physical Review Letters*, vol. 48, no. 26, p. 1867, 1982.
- [15] A. Vilenkin, “Cosmic strings and domain walls,” *Physics reports*, vol. 121, no. 5, pp. 263–315, 1985.
- [16] A. Derevianko and M. Pospelov, “Hunting for topological dark matter with atomic clocks,” *Nature Physics*, vol. 10, no. 12, pp. 933–936, 2014.
- [17] B. M. Roberts, G. Blewitt, C. Dailey, M. Murphy, M. Pospelov, A. Rollings, J. Sherman, W. Williams, and A. Derevianko, “Search for domain wall dark matter with atomic clocks on board global positioning system satellites,” *Nature communications*, vol. 8, no. 1, p. 1195, 2017.
- [18] T. Kalaydzhyan and N. Yu, “Extracting dark matter signatures from atomic clock stability measurements,” *Physical Review D*, vol. 96, no. 7, p. 075007, 2017.
- [19] D.-C. Dai, D. Minic, and D. Stojkovic, “Interaction of cosmological domain walls with large classical objects, like planets and satellites, and the flyby anomaly,” *Journal of High Energy Physics*, vol. 2022, no. 3, pp. 1–17, 2022.
- [20] Y. Stadnik and V. Flambaum, “Searching for topological defect dark matter via nongravitational signatures,” *Physical review letters*, vol. 113, no. 15, p. 151301, 2014.
- [21] S. Pustelny, D. F. Jackson Kimball, C. Pankow, M. P. Ledbetter, P. Włodarczyk, P. Wcisło, M. Pospelov, J. R. Smith, J. Read, W. Gawlik, *et al.*, “The global network of optical magnetometers for exotic physics (gnome): A novel scheme to search for physics beyond the standard model,” *Annalen der Physik*, vol. 525, no. 8-9, pp. 659–670, 2013.
- [22] S. Afach, B. C. Buchler, D. Budker, C. Dailey, A. Derevianko, V. Dumont, N. L. Figueroa, I. Gerhardt, Z. D. Grujić, H. Guo, *et al.*, “Search for topological defect dark matter with a global network of optical magnetometers,” *Nature Physics*, vol. 17, no. 12, pp. 1396–1401, 2021.

- [23] R. L. McNally and T. Zelevinsky, “Constraining domain wall dark matter with a network of superconducting gravimeters and ligo,” *The European Physical Journal D*, vol. 74, no. 4, p. 61, 2020.
- [24] E. D. Hall, R. X. Adhikari, V. V. Frolov, H. Müller, and M. Pospelov, “Laser interferometers as dark matter detectors,” *Physical Review D*, vol. 98, no. 8, p. 083019, 2018.
- [25] H. Grote and Y. Stadnik, “Novel signatures of dark matter in laser-interferometric gravitational-wave detectors,” *Physical Review Research*, vol. 1, no. 3, p. 033187, 2019.
- [26] J. Jaeckel, S. Schenk, and M. Spannowsky, “Probing dark matter clumps, strings and domain walls with gravitational wave detectors,” *The European Physical Journal C*, vol. 81, no. 9, p. 828, 2021.
- [27] P. G. Kevrekidis, I. Danaila, J.-G. Caputo, and R. Carretero-González, “Planar and radial kinks in nonlinear klein-gordon models: Existence, stability, and dynamics,” *Physical Review E*, vol. 98, no. 5, p. 052217, 2018.
- [28] R. Carretero-González, L. Cisneros-Ake, R. Decker, G. Koutsokostas, D. J. Frantzeskakis, P. Kevrekidis, and D. J. Ratliff, “Kink–antikink stripe interactions in the two-dimensional sine–gordon equation,” *Communications in Nonlinear Science and Numerical Simulation*, vol. 109, p. 106123, 2022.
- [29] J.-G. Caputo and M. P. Sørensen, “Radial sine-gordon kinks as sources of fast breathers,” *Physical Review E—Statistical, Nonlinear, and Soft Matter Physics*, vol. 88, no. 2, p. 022915, 2013.
- [30] J. Maldacena, “The large- $n$  limit of superconformal field theories and supergravity,” *International journal of theoretical physics*, vol. 38, no. 4, pp. 1113–1133, 1999.
- [31] E. Witten, “Anti de sitter space and holography,” *arXiv preprint hep-th/9802150*, 1998.
- [32] Z.-H. Li, H.-Q. Shi, and H.-Q. Zhang, “From black hole to one-dimensional chain: Parity symmetry breaking and kink formation,” *Physical Review D*, vol. 108, no. 10, p. 106015, 2023.
- [33] T.-C. Ma, H.-Q. Shi, H.-Q. Zhang, and A. del Campo, “Universal critical holography and domain wall formation,” *Physical Review Research*, vol. 7, no. 1, p. 013096, 2025.
- [34] H. Arodz, “Expansion in the width and collective dynamics of a domain wall,” *Nuclear Physics B*, vol. 509, no. 1-2, pp. 273–293, 1998.
- [35] T. Dobrowolski, “Construction of curved domain walls,” *Physical Review E—Statistical, Nonlinear, and Soft Matter Physics*, vol. 77, no. 5, p. 056608, 2008.
- [36] T. Dobrowolski, “Kink motion in a curved josephson junction,” *Physical Review E—Statistical, Nonlinear, and Soft Matter Physics*, vol. 79, no. 4, p. 046601, 2009.
- [37] J. Gatlik and T. Dobrowolski, “Modeling kink dynamics in the sine–gordon model with position dependent dispersive term,” *Physica D: Nonlinear Phenomena*, vol. 428, p. 133061, 2021.
- [38] C. Gorria, Y. B. Gaididei, M. P. Sørensen, P. L. Christiansen, and J. G. Caputo, “Kink propagation and trapping in a two-dimensional curved josephson junction,” *Physical Review B*, vol. 69, no. 13, p. 134506, 2004.
- [39] H.-Q. Shi, T.-C. Ma, and H.-Q. Zhang, “Topologically protected metastable states in classical dynamics,” *Chaos, Solitons & Fractals*, vol. 182, p. 114789, 2024.
- [40] R. Ruffini and J. A. Wheeler, “Introducing the black hole,” *Physics today*, vol. 24, no. 1, pp. 30–41, 1971.
- [41] V. Frolov and I. Novikov, *Black hole physics: Basic concepts and new developments*, vol. 96. Springer Science & Business Media, 2012.

- [42] J. M. Lattimer and M. Prakash, “The physics of neutron stars,” *science*, vol. 304, no. 5670, pp. 536–542, 2004.
- [43] J. M. Lattimer, “Neutron stars,” *General Relativity and Gravitation*, vol. 46, no. 5, p. 1713, 2014.
- [44] P. Jetzer, “Boson stars,” *Physics Reports*, vol. 220, no. 4, pp. 163–227, 1992.
- [45] F. E. Schunck and E. W. Mielke, “General relativistic boson stars,” *Classical and Quantum Gravity*, vol. 20, no. 20, p. R301, 2003.
- [46] S. W. Hawking, “Wormholes in spacetime,” *Physical Review D*, vol. 37, no. 4, p. 904, 1988.
- [47] M. S. Morris and K. S. Thorne, “Wormholes in spacetime and their use for interstellar travel: A tool for teaching general relativity,” *American Journal of Physics*, vol. 56, no. 5, pp. 395–412, 1988.
- [48] D.-C. Dai, D. Minic, and D. Stojkovic, “How to form a wormhole,” *The European Physical Journal C*, vol. 80, no. 12, p. 1103, 2020.
- [49] R. Moderski and M. Rogatko, “Thick domain walls and charged dilaton black holes,” *Physical Review D*, vol. 67, no. 2, p. 024006, 2003.
- [50] Y. Morisawa, D. Ida, A. Ishibashi, and K.-i. Nakao, “Thick domain walls around a black hole,” *Physical Review D*, vol. 67, no. 2, p. 025017, 2003.
- [51] R. Moderski and M. Rogatko, “Reissner-nordström black holes and thick domain walls,” *Physical Review D*, vol. 69, no. 8, p. 084018, 2004.
- [52] R. Moderski and M. Rogatko, “Thick domain walls in ads black hole spacetimes,” *Physical Review D—Particles, Fields, Gravitation, and Cosmology*, vol. 74, no. 4, p. 044002, 2006.
- [53] F. Ficek and P. Mach, “Planar domain walls in black hole spacetimes,” *Physical Review D*, vol. 97, no. 4, p. 044012, 2018.
- [54] J.-G. Caputo, T. Dobrowolski, J. Gatlík, and P. G. Kevrekidis, “Radial kinks in a schwarzschild-like geometry,” *Physical Review D*, vol. 110, no. 12, p. 125025, 2024.
- [55] T.-C. Ma, X.-Y. Wang, and H.-Q. Zhang, “Radial kinks in the boson stars,” *arXiv preprint arXiv:2510.13923*, 2025.
- [56] S. V. Sushkov and S.-W. Kim, “Wormholes supported by a kink-like configuration of a scalar field,” *Classical and Quantum Gravity*, vol. 19, no. 19, p. 4909, 2002.
- [57] P. Bizoń, M. Dunajski, M. Kahl, and M. Kowalczyk, “Sine-gordon on a wormhole,” *Nonlinearity*, vol. 34, no. 8, p. 5520, 2021.
- [58] B. A. Díaz Arias, “Kinks of the sine-gordon equation on a wormhole,” *Thesis in UNIVERSIDAD DE CHILE*, (2023) <https://repositorio.uchile.cl/bitstream/handle/2250/193976/Kinks-of-the-Sine-Gordon-equation-on-a-wormhole.pdf?sequence=1&isAllowed=y>.
- [59] A. Waterhouse, “The  $\phi^4$  kink on a wormhole spacetime,” *arXiv preprint arXiv:1908.09650*, 2019.
- [60] P. Goulart, “Phantom wormholes in einstein–maxwell-dilaton theory,” *Classical and Quantum Gravity*, vol. 35, no. 2, p. 025012, 2017.
- [61] A. Einstein and N. Rosen, “The particle problem in the general theory of relativity,” *Physical Review*, vol. 48, no. 1, p. 73, 1935.
- [62] H. G. Ellis, “Ether flow through a drainhole: A particle model in general relativity,” *Journal of Mathematical Physics*, vol. 14, no. 1, pp. 104–118, 1973.
- [63] M. S. Morris, K. S. Thorne, and U. Yurtsever, “Wormholes, time machines, and the weak energy condition,” *Physical Review Letters*, vol. 61, no. 13, p. 1446, 1988.
- [64] M. Chianese, E. Di Grezia, M. Manfredonia, and G. Miele, “Characterising exotic matter driving wormholes,” *The European Physical Journal Plus*, vol. 132, no. 4, p. 164, 2017.

- [65] E. Di Grezia, E. Battista, M. Manfredonia, and G. Miele, “Spin, torsion and violation of null energy condition in traversable wormholes,” *The European Physical Journal Plus*, vol. 132, no. 12, p. 537, 2017.
- [66] E. Battista, S. Capozziello, and A. Errehymy, “Generalized uncertainty principle corrections in rastall–rainbow casimir wormholes,” *The European Physical Journal C*, vol. 84, no. 12, p. 1314, 2024.
- [67] D.-C. Dai, D. Minic, and D. Stojkovic, “New wormhole solution in de sitter space,” *Physical Review D*, vol. 98, no. 12, p. 124026, 2018.
- [68] V. De Falco, E. Battista, S. Capozziello, and M. De Laurentis, “Reconstructing wormhole solutions in curvature based extended theories of gravity,” *The European Physical Journal C*, vol. 81, no. 2, p. 157, 2021.
- [69] V. De Falco, E. Battista, S. Capozziello, and M. De Laurentis, “Testing wormhole solutions in extended gravity through the poynting-robertson effect,” *Physical Review D*, vol. 103, no. 4, p. 044007, 2021.
- [70] V. De Falco, E. Battista, S. Capozziello, and M. De Laurentis, “General relativistic poynting-robertson effect to diagnose wormholes existence: static and spherically symmetric case,” *Physical Review D*, vol. 101, no. 10, p. 104037, 2020.
- [71] D.-C. Dai and D. Stojkovic, “Observing a wormhole,” *Physical Review D*, vol. 100, no. 8, p. 083513, 2019.
- [72] C. Bambi and D. Stojkovic, “Astrophysical wormholes,” *Universe*, vol. 7, no. 5, p. 136, 2021.
- [73] C. De Simone, V. De Falco, and S. Capozziello, “Can wormholes mirror the quasinormal mode spectrum of schwarzschild black holes?,” *Physical Review D*, vol. 111, no. 6, p. 064021, 2025.
- [74] V. De Falco, M. De Laurentis, and S. Capozziello, “Epicyclic frequencies in static and spherically symmetric wormhole geometries,” *Physical Review D*, vol. 104, no. 2, p. 024053, 2021.
- [75] V. De Falco and S. Capozziello, “Static and spherically symmetric wormholes in metric-affine theories of gravity,” *arXiv preprint arXiv:2308.05440*, 2023.
- [76] A. Simpson and M. Visser, “Black-bounce to traversable wormhole,” *Journal of Cosmology and Astroparticle Physics*, vol. 2019, no. 02, p. 042, 2019.
- [77] T. W. Kibble, “Some implications of a cosmological phase transition,” *Physics Reports*, vol. 67, no. 1, pp. 183–199, 1980.
- [78] W. H. Zurek, “Cosmological experiments in superfluid helium?,” *Nature*, vol. 317, no. 6037, pp. 505–508, 1985.
- [79] T.-C. Ma, H.-Q. Shi, and H.-Q. Zhang, “Asymmetric symmetry breaking: Unequal probabilities of vacuum selection,” *arXiv preprint arXiv:2405.05168*, 2024.
- [80] E. J. Weinberg, “Classical solutions in quantum field theories,” *Ann. Rev. Nucl. Part. Sci.*, vol. 42, pp. 177–210, 1992.